

Electronic structures of normal and inverse spinel ferrites from first principlesZ. Szotek,¹ W. M. Temmerman,¹ D. Ködderitzsch,² A. Svane,³ L. Petit,⁴ and H. Winter⁵¹*Daresbury Laboratory, Daresbury, Warrington, WA4 4AD, Cheshire, United Kingdom*²*Physikalische Chemie, Ludwig-Maximilian University, Munich, Germany*³*Department of Physics and Astronomy, University of Aarhus, DK-8000 Aarhus C, Denmark*⁴*Computer Science and Mathematics Division, and Center for Computational Sciences, Oak Ridge National Laboratory, Oak Ridge, Tennessee 37831, USA*⁵*IFP, Forschungszentrum Karlsruhe GmbH, Postfach 3640, D-76021 Karlsruhe, Germany*

(Received 22 May 2006; revised manuscript received 2 October 2006; published 28 November 2006)

We apply the self-interaction corrected local spin density approximation to study the electronic structure and magnetic properties of the spinel ferrites MnFe_2O_4 , Fe_3O_4 , CoFe_2O_4 , and NiFe_2O_4 . We concentrate on establishing the nominal valence of the transition metal elements and the ground state structure, based on the study of various valence scenarios for both the inverse and normal spinel structures for all the systems. For both structures we find all the studied compounds to be insulating, but with smaller gaps in the normal spinel scenario. On the contrary, the calculated spin magnetic moments and the exchange splitting of the conduction bands are seen to increase dramatically when moving from the inverse spinel structure to the normal spinel kind. We find substantial orbital moments for NiFe_2O_4 and CoFe_2O_4 .

DOI: [10.1103/PhysRevB.74.174431](https://doi.org/10.1103/PhysRevB.74.174431)

PACS number(s): 75.50.Gg

I. INTRODUCTION

The field of spintronics is concerned with search for highly spin-polarized materials. One aim is to enhance tunnelling magnetoresistance (TMR) of magnetic tunnel junctions (MTJs) which are active members of magnetic random access memory (MRAM) elements. Also, the highly spin-polarized materials are of paramount importance for increasing spin-polarization of currents injected into semiconductors, required for an optimal operation of spintronics devices.¹ There appears to be a number of ways to achieve high spin-polarization, most notably by employing fully spin-polarized ferromagnetic metals, namely half-metals (HM).² Another possibility is to exploit features of the band structure of such tunnel barrier materials as, e.g., MgO, and filtering electronic wave functions according to their symmetry in order to select the most highly spin-polarized ones.^{3,4} The least explored possibility is exploiting the spin-filtering effect, based on ferromagnetic or ferrimagnetic insulating barriers. It was introduced by Moodera *et al.*,⁵ using EuS tunnel barriers. Spin filtering effect has been demonstrated in Gd/EuS/Al junctions,⁶ which exhibit high magnetoresistance, but show no great prospects for technological applications, on account of the low Curie temperature, T_c , of EuS.

Spinel ferrites⁷ have been studied for many years both regarding their magnetic behavior and correlated nature in conjunction with their structural properties to increase their performance in high-frequency devices. Some of them can probably be used as spin filters. Spin-dependent gap should result in spin-dependent barrier for tunnelling of electrons through the insulator, giving rise to spin filtering. Since the tunnelling probability depends exponentially on the barrier height, the spin filtering efficiency can be very high. Candidates for spin filters include such spinel ferrites as NiFe_2O_4 , CoFe_2O_4 , and MnFe_2O_4 .⁸ In particular, recently a spin filtering efficiency of up to 22% by the NiFe_2O_4 barrier has been reported by Lüders *et al.*^{9,10} In addition, Lüders *et al.*^{11,12}

have demonstrated TMR of 120% in $\text{La}_{2/3}\text{Sr}_{1/3}\text{MnO}_3/\text{SrTiO}_3/\text{NiFe}_2\text{O}_4$ junctions, which corresponds to 45% spin polarization for the conductive NiFe_2O_4 film, which stays constant up to about 300 K.

These spinel ferrites belong to the same family as magnetite (Fe_3O_4) which has been most thoroughly studied both for its HM character and the famous charge order.^{13,14} Many theoretical studies have been dedicated to magnetite, and in particular its charge order (which will not be discussed in the present paper) using various approximations to density functional theory (DFT) such as local spin density (LSD) approximation or generalized gradient approximation (GGA), as well as going beyond, for example, by invoking the Hubbard U through the LDA+ U (local density approximation + U) approach, or using the self-interaction corrected (SIC)-LSD method.^{15–20} For the other spinel ferrites most theoretical studies have been done with LSD, GGA,^{8,21–23} LDA+ U (Ref. 24) or hybrid density functionals.²⁵ The former two approaches usually describe these materials to be half-metallic and not insulating, if no distortions are included. The reason is that the transition metal (TM) d electrons in oxides (as well as f electrons in rare earth compounds) are strongly correlated and cannot be adequately described within the standard band theory framework with such approximations as LSD or GGA, placing them too high in energy around the Fermi level. The LDA+ U approach, treating the Hubbard U as an adjustable parameter, has correctly described CoFe_2O_4 and NiFe_2O_4 as insulators, but MnFe_2O_4 as a half-metal,²⁴ similarly to LSD and GGA. The SIC-LSD method,²⁶ which is parameter free, provides better description of correlations than LSD, and has been successfully applied to a variety of d - and f -electron materials.^{27–29} In this paper we apply the SIC-LSD approximation to study the electronic structure of spinel transition metal oxides MnFe_2O_4 , Fe_3O_4 , CoFe_2O_4 , and NiFe_2O_4 . We concentrate on the nominal valence of the TM elements and electronic and magnetic properties of these systems in both normal and in-

verse spinel structures. The reason being that in most cases these materials appear to exist as some mixture of those structures.

The paper is organized as follows. An overview of the basic features of the SIC-LSD formalism is presented in the next section. Section III gives some computational details, while the results of the application of the SIC-LSD method to the spinel ferrites $TMFe_2O_4$ (where TM represents Mn, Fe, Co, and Ni), are presented and discussed in Sec. IV. The paper is concluded in Sec. V.

II. THEORY

The basis of the SIC-LSD formalism is a self-interaction free total energy functional, E^{SIC} , obtained by subtracting from the LSD total energy functional, E^{LSD} , a spurious self-interaction of each occupied electron state ψ_α ,³⁰ namely

$$E^{\text{SIC}} = E^{\text{LSD}} - \sum_{\alpha}^{\text{occ}} \delta_{\alpha}^{\text{SIC}}. \quad (1)$$

Here α numbers the occupied states and the self-interaction correction for the state α is

$$\delta_{\alpha}^{\text{SIC}} = U[n_{\alpha}] + E_{xc}^{\text{LSD}}[\bar{n}_{\alpha}], \quad (2)$$

with $U[n_{\alpha}]$ being the Hartree energy and $E_{xc}^{\text{LSD}}[\bar{n}_{\alpha}]$ the LSD exchange-correlation energy for the corresponding charge density n_{α} and spin density \bar{n}_{α} . It is the LSD approximation to the exact exchange-correlation energy functional which gives rise to the spurious self-interaction. The exact exchange-correlation energy E_{xc} has the property that for any single electron spin density, \bar{n}_{α} , it cancels exactly the Hartree energy, thus

$$U[n_{\alpha}] + E_{xc}[\bar{n}_{\alpha}] = 0. \quad (3)$$

In the LSD approximation this cancellation does not take place, and for well localized states the above sum can be substantially different than zero. For extended states in periodic solids the self-interaction vanishes.

The SIC-LSD approach can be viewed as an extension of LSD in the sense that the self-interaction correction is only finite for spatially localized states, while for Bloch-type single-particle states E^{SIC} is equal to E^{LSD} . Thus, the LSD minimum is also a local minimum of E^{SIC} . A question now arises, whether there exist other competitive minima, corresponding to a finite number of localized states, which could benefit from the self-interaction term without losing too much of the energy associated with band formation. This is often the case for rather well localized electrons like the $3d$ electrons in transition metal oxides or the $4f$ electrons in rare earth compounds. It follows from minimization of Eq. (1) that within the SIC-LSD approach such localized electrons move in a different potential than the delocalized valence electrons which respond to the effective LSD potential. Thus, by including an explicit energy contribution for an electron to localize, the *ab initio* SIC-LSD describes both localized and delocalized electrons on an equal footing, leading to a greatly improved description of correlation effects over the LSD approximation, as well as, to determination of valence.

In order to make the connection between valence and localization more explicit, it is useful to define the nominal valence²⁹ as

$$N_{\text{val}} = Z - N_{\text{core}} - N_{\text{SIC}},$$

where Z is the atomic number (26 for Fe), N_{core} is the number of core (and semicore) electrons (18 for Fe), and N_{SIC} is the number of localized, i.e., self-interaction corrected, states (either five or six, respectively, for Fe^{3+} and Fe^{2+}). Thus, in this formulation the valence is equal to the integer number of electrons available for band formation. The localized electrons do not participate in bonding. To find the nominal valence we assume various atomic configurations, consisting of different numbers of localized states, and minimize the SIC-LSD energy functional of Eq. (1) with respect to the number of localized electrons.

The SIC-LSD formalism is governed by the energetics due to the fact that for each orbital the SIC differentiates between the energy gain due to hybridization of the orbital with the valence bands and the energy gain upon localization of the orbital. Whichever wins determines if the orbital is part of the valence band or not, and in this manner also leads to the evaluation of the valence of elements involved. The SIC depends on the choice of orbitals and its value can differ substantially as a result of this. Therefore, one must be guided by the energetics in defining the most optimally localized orbitals to determine the absolute energy minimum of the SIC-LSD energy functional. The advantage of the SIC-LSD formalism is that for such systems as transition metal oxides or rare earth compounds the lowest energy solution will describe the situation where some single-electron states may not be of Bloch-type form. Specifically, in oxides, Mn-, Co-, Ni-, and Fe- $3d$ states may be assumed to be localized, but not the O $2p$ states, because treating them as localized is energetically unfavorable.

The SIC-LSD approach has been implemented²⁶ within the linear muffin-tin-orbital (LMTO) atomic sphere approximation (ASA) band structure method,³¹ in the tight-binding representation.³² In this method the polyhedral Wigner Seitz cell is approximated by slightly overlapping atom centered spheres, with a total volume equal to the actual crystal volume, while the electron wave functions are expanded in terms of the screened muffin-tin orbitals, and the minimization of E^{SIC} becomes nonlinear in the expansion coefficients. The so-called combined correction term³³ has been implemented and consistently applied to improve on the ASA.

III. COMPUTATIONAL DETAILS

The spinel ferrites of interest to the present study have a general chemical formula of the form AB_2O_4 and crystallize in the face-centred-cubic structure. In the normal spinel structure A is a divalent element atom, occupying tetrahedral A sites, while B is a trivalent element, sitting on the octahedral B sites. When A is a trivalent element, and B consists of equal numbers of divalent and trivalent elements, distributed over crystallographically equivalent $B1$ and $B2$ octahedral sites, then the spinel structure is referred to as the inverse kind. In TM ferrites substantial off-stoichiometry and inter-

TABLE I. The lattice constants (a) and corresponding ASA radii (r_{ASA}) for the transition metal elements occupying tetrahedral (tet) and octahedral (oct) sites, and for oxygen ions (in atomic units) for all the studied spinel ferrites. The radii of the empty spheres used in the calculations are not given, although typically four to five different types were used, all of the order of 1.65–1.95 atomic units, depending on the system, however, never exceeding the size of the oxygen spheres.

System	a	$r_{\text{ASA}}^{\text{tet}}$	$r_{\text{ASA}}^{\text{oct}}$	$r_{\text{ASA}}^{\text{O2}}$	$r_{\text{ASA}}^{\text{O2}}$
MnFe ₂ O ₄	16.08	2.204	2.588	1.979	1.979
Fe ₃ O ₄	15.87	2.329	2.752	1.848	1.848
CoFe ₂ O ₄	15.84	2.434	2.696	1.928	1.928
NiFe ₂ O ₄	15.78	2.425	2.686	1.920	1.920

site disorder are often present in samples, but are not considered in this paper. The high temperature phase of magnetite is known to have the inverse spinel structure, where A atoms are Fe³⁺ ions, and B sites are equally populated by Fe²⁺ and Fe³⁺ ions. Similarly, the NiFe₂O₄ system has been established experimentally to crystallize in the inverse spinel structure, with the A sites being Fe³⁺ ions, while B sites equally populated by Ni²⁺ and Fe³⁺ ions. The MnFe₂O₄, on the other hand, is considered to be predominantly of the normal spinel kind, as about 80% of A sites are populated by Mn²⁺ ions.^{7,34} The CoFe₂O₄ material is considered to be mostly an inverse spinel compound with about 80% of divalent Co ions occupying octahedral sites.^{7,35,36} As the experimental situation with respect to the observed structures and TM valences is not fully established, and the computer simulation of the exact physical conditions is very difficult, in this paper we study both extremes, namely the normal and inverse spinel structures for all the systems. In addition, we investigate a number of different valence scenarios, defined in the following sections, to find the most energetically favorable solutions, be it only at zero temperature, for all the studied systems.

Regarding the magnetic structure of the ferrites, we assume that of magnetite, with the spins of the TM atoms on the tetrahedral sublattice being antiparallel to those of the octahedral sublattice. Within a given sublattice the spins of all the TM atoms are arranged in parallel to one another.

The calculations have been performed for the experimental lattice parameters, whose values, together with the corresponding ASA radii, are given in Table I.⁸ For the basis functions, we have used s -, p -, and d -muffin-tin orbitals on all the transition metal atoms as the so-called low waves and on the oxygen the s and p orbitals have been treated as low waves and the d orbitals have been downfolded.³⁷ For a better space filling and to increase the number of basis functions, a set of empty spheres has also been included in the calculations. For the empty spheres only the s basis functions have been treated as low waves, while both p and d orbitals have been downfolded. All the calculations have been performed in the scalar-relativistic mode, but for the calculated ground state configurations the spin-orbit coupling (SOC) was also included to calculate the orbital moment, in addition to the spin moment.

IV. RESULTS AND DISCUSSION

A. MnFe₂O₄

As mentioned earlier, this compound is believed to be of predominantly normal spinel character. It is insulating, with a small gap of 0.04–0.06 eV as determined by transport experiments.³⁸ Our calculations have addressed the important issues of this system by realizing both normal (N) and inverse (I) spinel arrangements of ions on the tetrahedral and octahedral sites. In addition, the all 3+ scenario, where all the sites are occupied exclusively by the 3+ ions, has also been studied. Note that in the normal spinel environment the latter would mean that Mn³⁺ (four d electrons are considered as localized) ions occupy the tetrahedral sites, while all the octahedral sites are exclusively populated by Fe³⁺ ions ($N3+$ scenario). For the inverse spinel environment the tetrahedral ions would be of Fe³⁺ type, with the $B1$ octahedral sites occupied by Mn³⁺ ions and the $B2$ sites by Fe³⁺ ions ($I3+$ scenario). In Table II, we summarize the total energy differences for all the scenarios studied for MnFe₂O₄, in comparison with all the other spinel ferrites.

We find the normal spinel arrangement of ions to be the calculated ground state for MnFe₂O₄ (Table II), in agreement with the experimental evidence for predominantly normal spinel character of this compound. The ground state solution is followed closely by the all 3+ scenario, realized in the normal spinel environment ($N3+$), which lies only 0.28 eV higher in energy. The inverse spinel solution is 0.58 eV higher, while the $I3+$ scenario is the most unfavorable state for MnFe₂O₄.

To establish whether the degree of localization of d electrons of the TM ions residing on the tetrahedral sites has any bearing on the preference towards normal spinel structure in MnFe₂O₄, we have looked at the change in the localization energy when switching Mn²⁺ ion between the tetrahedral and octahedral sites. We have found that the localization energy associated with Mn²⁺ on the tetrahedral sites is 0.15 eV smaller than when Mn²⁺ ions occupy the octahedral sites. At the same time the localization energy associated with the Fe³⁺ ions is smaller by 0.19 eV for the tetrahedral sites, in comparison with the situation when on the octahedral sites. Hence, the localization energy alone favors the normal spinel structure only by 0.04 eV over the inverse spinel kind, which constitutes just a tiny fraction of the total energy difference of 0.58 eV (Table II). Thus, the preference of MnFe₂O₄ for

TABLE II. Total energy differences (in eV per formula unit), calculated within SIC-LSD, between the ground state configuration and other valence and/or structure scenarios for all studied spinel ferrites at the experimental lattice constant. The row marked by N means normal spinel arrangement, where the tetrahedral sites are occupied by the divalent ions, namely Mn^{2+} in $MnFe_2O_4$ compound, Fe^{2+} in Fe_3O_4 , Co^{2+} in $CoFe_2O_4$ and finally Ni^{2+} in $NiFe_2O_4$, while the octahedral sites are populated exclusively by Fe^{3+} ions. Similarly, the row marked by I means that the $B1$ sites are occupied by Mn^{2+} in $MnFe_2O_4$, Fe^{2+} in Fe_3O_4 , Co^{2+} in $CoFe_2O_4$ and Ni^{2+} in $NiFe_2O_4$, with all the tetrahedral and $B2$ octahedral sites taken by the Fe^{3+} ions. The notation $I3+$ means that tetrahedral sites and $B2$ octahedral sites in all the compounds are occupied by Fe^{3+} ions, while the $B1$ octahedral sites are populated by Mn^{3+} ions in $MnFe_2O_4$, Fe^{3+} ions in Fe_3O_4 , Co^{3+} ions in $CoFe_2O_4$, and Ni^{3+} ions in $NiFe_2O_4$. In the $N3+$ scenario all the octahedral sites, in all the compounds studied, are occupied by the Fe^{3+} ions, and the tetrahedral sites are taken by Mn^{3+} ions in $MnFe_2O_4$, Fe^{3+} ions in Fe_3O_4 , Co^{3+} ions in $CoFe_2O_4$, and Ni^{3+} ions in $NiFe_2O_4$. Note, that in the Fe_3O_4 case the latter two scenarios, namely $N3+$ and $I3+$, are equivalent.

Scenario	$MnFe_2O_4$	Fe_3O_4	$CoFe_2O_4$	$NiFe_2O_4$
I	0.58	1.54	0.20	0.00
$I3+$	0.92	0.00	0.00	0.52
N	0.00	2.46	1.09	1.66
$N3+$	0.28	0.00	0.46	1.57

the normal spinel structure is mostly driven by other electronic degrees of freedom.

Regarding the density of states (DOS) of $MnFe_2O_4$ in the calculated ground state normal spinel structure (the top panel of Fig. 1), one can see that it is insulating, with a gap of about 0.075 eV which compares rather well with the experimental value obtained from transport measurements.³⁸ A larger gap of about 0.3 eV is calculated for $MnFe_2O_4$ in the inverse spinel structure (bottom panel of Fig. 1), but the spin splitting of the conduction band is here considerably smaller than for the ground state normal spinel scenario (Table III). In variance to the normal and inverse spinel cases, the $N3+$ scenario (center panel) is found to be half-metallic.

Compared to the SIC-LSD band gap, other approaches give either much larger gaps or find $MnFe_2O_4$ to be a half-metal, as seen in Table IV. It is clear from the table, that besides the present calculations only the hybrid functional approach finds an insulating ground state for $MnFe_2O_4$. However, the gap of the latter approach depends strongly on the weighting factor, w , with which the exact exchange is included into the calculation. As a result, changing this weighting factor from 40% to 100% increases the band gap from over 4.0 eV to over 13.0 eV,²⁵ which is at least two orders of magnitude larger than the experiment finds. The LDA+ U study,²⁴ with U of 4.0 eV for Mn^{2+} ions and U of

TABLE III. Spin decomposed exchange splittings of the valence and conduction bands, as well as the energy gaps (in eV), for both inverse and normal spinel structures for $MnFe_2O_4$. Here VBM stands for the valence band maximum and CBM for the conduction band minimum, and \uparrow refers to spin-up and \downarrow to spin-down component.

	I scenario	N scenario
VBM \uparrow -VBM \downarrow	0.69	-0.91
CBM \uparrow -CBM \downarrow	1.31	3.85
CBM \uparrow -VBM \uparrow	1.64	4.84
CBM \downarrow -VBM \downarrow	1.02	0.075
Gap	0.33	0.075

4.5 eV for Fe^{2+} ions, has not delivered an insulating ground state for $MnFe_2O_4$. Similarly, the LSD and GGA calculations have obtained a half-metallic solutions, but in the case of GGA the authors of Ref. 23 claim that this compound is a complex insulator. Although they describe $MnFe_2O_4$ as a low carrier density half-metal in the stoichiometric structure, there are indications that insulating character may arise upon interchange of Mn and Fe atoms. Thus, they envisage to open up an insulating gap using Anderson localization mechanism, associated with the intersite Mn-Fe disorder.

For all the scenarios studied with SIC-LSD, the valence band of $MnFe_2O_4$ is predominantly of the oxygen type, with a very small admixture of the TM character, and its polarization at the top of the band changes from positive to negative between the inverse and normal spinel scenarios (Table III). What also changes substantially when moving from the normal to inverse spinel scenario is the conduction band splitting, which for the normal spinel scenario is about 2.5 eV larger than that of the inverse spinel case. The reason being that the unoccupied TM d states are substantially pushed up in energy when in the normal spinel environment. Considering that in reality $MnFe_2O_4$ is not a pure normal spinel compound, the exchange splitting of the conduction bands is most likely to be somewhere in between the values calculated for the normal and inverse spinel scenarios. Of course,

TABLE IV. Comparison of the types of ground state and energy gap for $MnFe_2O_4$ from different approaches: LSD (Ref. 8), GGA (Ref. 23), LDA+ U (Ref. 24), hybrid functionals (Ref. 25), and SIC-LSD (normal spinel scenario, present work). The experimental values come from transport experiment (Ref. 38).

Method	Type of ground state	Gap (eV)
LSD	Half-metal	
GGA	Half-metal	
LDA+ U	Half-metal	
Hybrid	Insulator	~4.0–13.0
SIC-LSD	Insulator	0.075
Experiment	Insulator	0.04–0.06

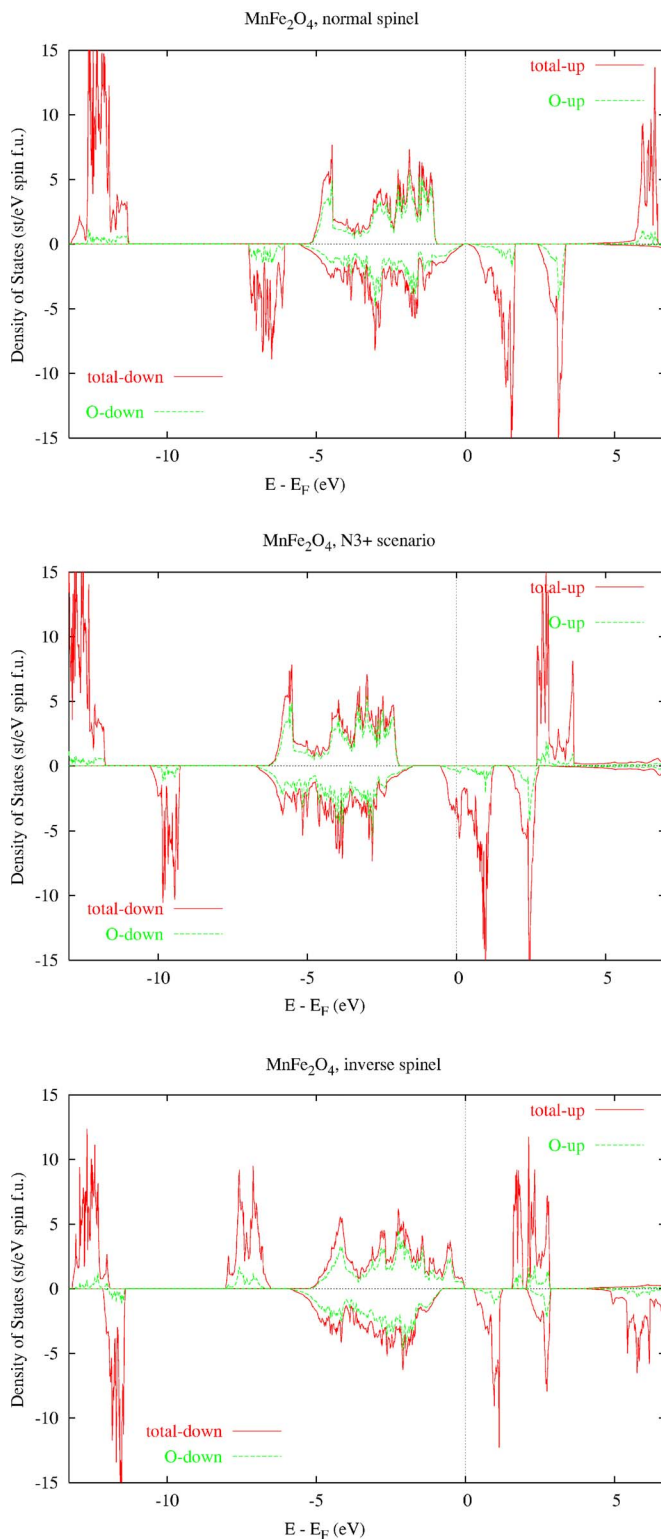


FIG. 1. (Color online) Spin decomposed total densities of states (in red), per formula unit, for MnFe_2O_4 for the normal spinel structure (N) (top), for the all 3+ scenario in the normal spinel arrangement of atoms ($N3+$) (center), and for the inverse spinel scenario (I) (bottom). The oxygen contribution to the total density of states is also shown (green, dotted lines). The minority DOS is printed on the negative side of the y-axis, while the majority contributions are presented on the positive side of this axis.

the larger the splitting, the more advantageous should it be for the spin filtering properties.

To understand details of the densities of states shown in Fig. 1, associated with the localized TM states, one should keep in mind that in the normal spinel scenario (top panel) which, as already been mentioned, is the calculated ground state structure for this compound, the tetrahedral sublattice is populated by Mn^{2+} ions and that in this case five minority Mn d electrons are described as localized states, seen just below the predominantly O $2p$ valence band, at about -6 eV. The unoccupied, majority Mn d electrons give rise to the states seen as peaks above the Fermi energy at about $+6$ eV. The octahedral sublattice is populated by Fe^{3+} ions, with five majority d electrons localized, as the two sublattices are antiparallel to one another. As a result the localized majority d Fe states are seen at about -12 eV below the Fermi energy. The unoccupied Fe d states, the minority ones, are seen just above the Fermi energy, over the range of up to about 3.5 eV.

In the $N3+$ scenario (center panel), one minority Mn d electron gets delocalized to realize Mn^{3+} ions on the tetrahedral sites. As a result the localized, minority Mn d peak has moved down in energy, lying just above -10 eV, while the fifth, now delocalized, minority d electron appears at the Fermi energy, bringing down also the unoccupied, minority, Fe d states. The situation changes in the inverse spinel scenario (bottom panel), as now Mn^{2+} ions reside on $B1$ sites of the octahedral sublattice, while the Fe^{3+} ions populate the tetrahedral sublattice and $B2$ sites of the octahedral sublattice. Thus on the tetrahedral sites we have five minority Fe d electrons which give rise to the peak at about -12 eV, while the localized Fe d electrons of the octahedral sublattice are seen as the peak on the majority side, at about -14 eV. The five localized Mn majority d states are again seen just below the valence band at about -7 eV. The unoccupied Mn minority d bands are seen at about 6 eV above the Fermi energy. The five unoccupied, majority, Fe d states, associated with the tetrahedral sublattice, are seen at about 2.5 eV above the Fermi energy. Finally, the unoccupied, minority, Fe d states of the octahedral sublattice are seen as two separate peaks above the Fermi energy. Note, however, that the SIC-LSD eigenvalues have no direct physical interpretation as removal energies, and thus should not be directly compared with spectroscopies. To do so, one would need to take into account relaxation/screening effects that are not included in such an effective one-electron theory as SIC-LSD. One way to accomplish this is to employ the Δ_{SCF} calculations,^{39–43} and another is the SIC-LSD based optimized effective potential (OEP) method.^{41,44–46}

The magnetic properties change when moving from the normal to inverse spinel scenario, as seen in Table V, where we compare the total spin magnetic moments for all the studied spinel ferrites. The total spin magnetic moment for MnFe_2O_4 is $5\mu_B$ per formula unit, for both insulating and half-metallic solutions, while for the metallic $I3+$ scenario the spin moment is reduced to $4.1\mu_B$ per formula unit. Note that unlike in the other ferrites there is no change in the total spin magnetic moment between the normal and inverse spinel scenarios. The reason being that, as seen in Table VI, there are only very small changes in the values of the spin

TABLE V. Total spin magnetic moments (in μ_B per formula unit), calculated within SIC-LSD, for all the studied spinel ferrites and scenarios.

Scenario	MnFe ₂ O ₄	Fe ₃ O ₄	CoFe ₂ O ₄	NiFe ₂ O ₄
<i>I</i>	5.00	4.00	3.00	2.00
<i>I3+</i>	4.10	4.00	3.00	2.00
<i>N</i>	5.00	6.00	7.00	8.00
<i>N3+</i>	5.00	4.00	5.60	6.80

moments of the transition metal ions, that are compensated by changes in the induced oxygen spin moments.

Including spin-orbit coupling for the ground state normal spinel scenario for MnFe₂O₄ compound, we find no considerable orbital moments either on Mn ($-0.0005\mu_B$) or on Fe ions ($0.019\mu_B$). As a result, the total orbital moment is of the order of $0.045\mu_B$ per formula unit, while at the same time the total spin moment is changed from $5.0\mu_B$ to $4.9995\mu_B$ per formula unit. Also, even with SOC included, we still observe a small energy gap of 0.064 eV, which incidently is in very good agreement with the transport experiments.³⁸

B. Fe₃O₄

Based upon its high magnetoresistive properties, magnetite is of interest for technological applications, as, e.g., computer memory, magnetic recording, etc. Magnetite is thought to be half-metallic, with the highest known T_c of 860 K. At about $T_V=122$ K it undergoes a transition to an insulating state, associated with some kind of charge order, setting in on the octahedral sites, and a distortion of the crystal structure from the inverse spinel cubic to monoclinic.^{13,14,47} Verwey argued that below the transition temperature, T_V , the Fe³⁺ and Fe²⁺ cations order in the alternate (001) planes, and interpreted this transition as an electron localization-delocalization transition.¹³

In the earlier paper, we have studied three different types of charge order on the octahedral sites, both in the high temperature (cubic) and low temperature (monoclinic) phases.²⁰ In this paper, for the sake of comparison with other spinel *TM* oxides, we concentrate exclusively on the high temperature cubic phase and the scenarios enumerated in Table V.

As seen from Table II and Fig. 2 (center panel), the ground state of magnetite in the cubic phase is half-metallic,

TABLE VI. Type-decomposed spin magnetic moments (in μ_B per formula unit), calculated within SIC-LSD, for MnFe₂O₄ for inverse and normal spinel structures. Here *A* marks the tetrahedral, while *B1* and *B2* mark the octahedral sites, and O1 and O2 stand for two different types of oxygens.

Scenario	Fe _A ³⁺	Mn _{B1} ²⁺	Fe _{B2} ³⁺	O1	O2
<i>I</i>	-4.09	4.58	4.11	0.12	0.03
Scenario	Mn _A ²⁺	Fe _{B1} ³⁺	Fe _{B2} ³⁺	O1	O2
<i>N</i>	-4.49	4.11	4.11	0.34	0.34

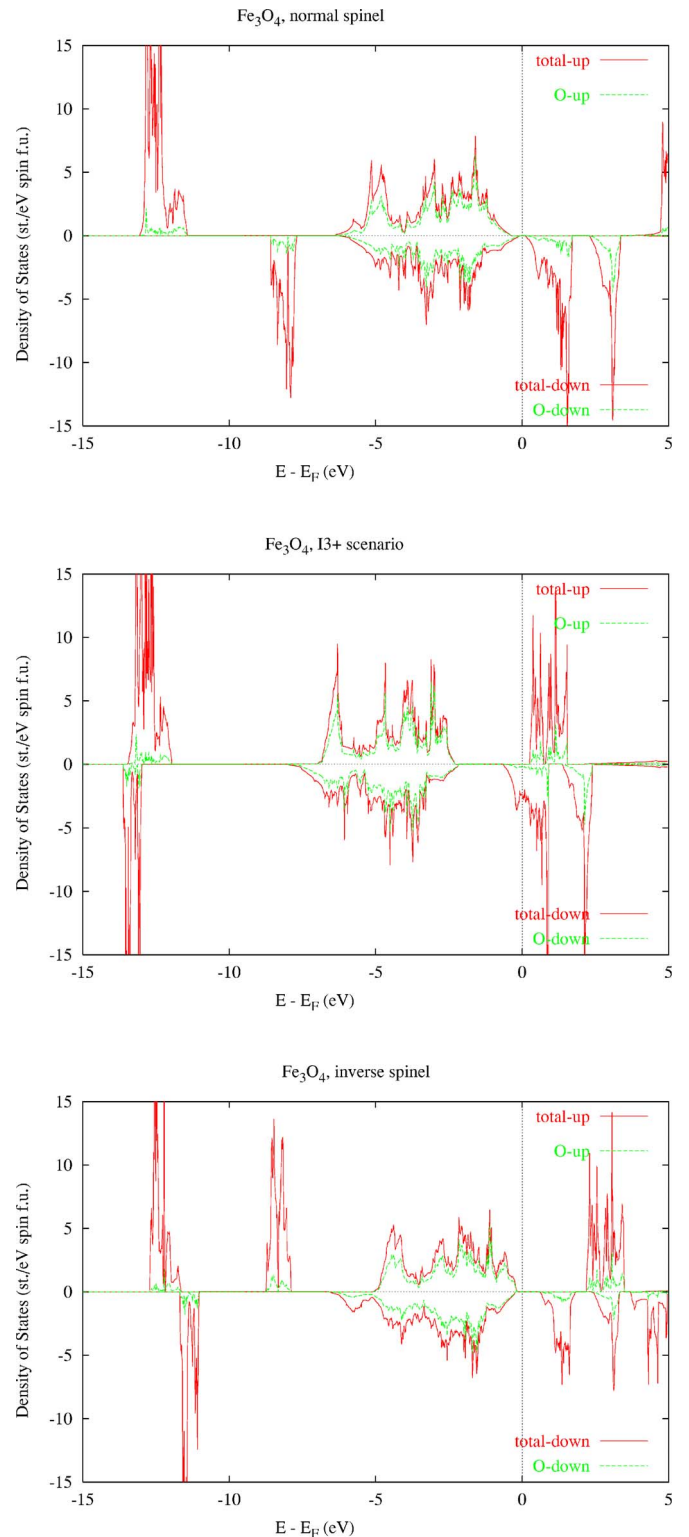


FIG. 2. (Color online) Spin decomposed total densities of states (in red), per formula unit, for Fe₃O₄ for the normal spinel structure (*N*) (top), for the all 3+ scenario in the inverse spinel arrangement of atoms (*I3+*) (center), and for the inverse spinel scenario (*I*) (bottom). The oxygen contribution to the total density of states is also shown (green dotted lines). The minority DOS is printed on the negative side of the y axis, while the majority contribution is shown on the positive side of this axis.

TABLE VII. Spin decomposed exchange splittings of the valence and conduction bands, as well as the energy gaps (in eV), for both inverse and normal spinel structures for Fe_3O_4 . Here VBM stands for the valence band maximum and CBM for the conduction band minimum, and \uparrow refers to spin-up and \downarrow to spin-down component.

	<i>I</i> scenario	<i>N</i> scenario
VBM \uparrow -VBM \downarrow	0.06	-0.35
CBM \uparrow -CBM \downarrow	1.61	3.65
CBM \uparrow -VBM \uparrow	2.33	4.08
CBM \downarrow -VBM \downarrow	0.78	0.08
Gap	0.72	0.08

with all Fe ions in 3+ configuration (five d electrons localized). This ground state scenario ($I3+ \equiv N3+$) is the result of a delocalization of the sixth d electron of the original Fe^{2+} ions, that together with Fe^{3+} ions randomly populate the octahedral $B1$ and $B2$ sites in the high-temperature cubic phase. In the ground state scenario, this sixth electron is seen to give rise to the peak at the Fermi energy in the minority channel, together with the other 10 unoccupied minority d states associated with the octahedral sites. The five localized tetrahedral Fe_A minority d states appear around -13 eV, while the unoccupied majority Fe_A d states are seen just above the Fermi energy. All the localized majority d states of the octahedral sites are at about -12.5 eV. The valence band is of predominantly $O p$ character.

The inverse spinel solution (Table II and the bottom panel of Fig. 2), corresponding to the assumed Verwey charge order, lies about 1.5 eV above the ground state. In this scenario, the above-mentioned sixth electron is localized on the $B1$ -octahedral sites, and appears as a small hump at the bottom of the minority valence band. The remaining five d states of the Fe_{B1} sites are seen at about -8 eV below the Fermi energy in the majority bands. The five localized majority Fe_{B2} d states lie at about -12.5 eV. The minority Fe_A d states (seen below -10 eV) are localized, and the majority Fe_A d states are unoccupied, occurring at about 3 eV above the Fermi energy. As a result, since the four remaining minority Fe_{B1} d states and five minority Fe_{B2} states are also unoccupied, our calculations for this scenario give an insulating state with a gap of ~ 0.7 eV. Understandably, as the latter has been calculated for the high-temperature inverse spinel structure, its value is much larger than the experimental value of 0.14 eV,⁴⁸ measured for the true, low temperature monoclinic phase.⁴⁹

Our calculations for the normal spinel structure give the most energetically unfavorable solution for magnetite, lying about 2.5 eV above the $I3+$ ground state scenario. In this normal spinel case (top panel of Fig. 2), we obtain an insulating solution with an energy gap of 0.08 eV. Here, the tetrahedral sites are occupied by Fe^{2+} ions, while the octahedral sites are populated with Fe^{3+} ions. As a result, five localized minority Fe_A d states lie at about -8 eV, while the sixth localized, majority, Fe_A d state sits right at the bottom of the majority valence band. All the remaining unoccupied majority Fe_A d states are just about seen at 5 eV above the Fermi

TABLE VIII. Total and type-decomposed spin magnetic moments (in Bohr magnetons per formula unit) for magnetite as calculated within SIC-LSD for three different scenarios. Only different Fe types are listed in the table.

Scenario	M_{total}	$M_{\text{Fe}_A^{2+}}$	$M_{\text{Fe}_A^{3+}}$	$M_{\text{Fe}_{B1}^{2+}}$	$M_{\text{Fe}_{B1}^{3+}}$	$M_{\text{Fe}_{B2}^{3+}}$
<i>I</i>	4.00		-4.00	3.57		4.08
<i>I3+</i>	4.00		-4.02		3.90	3.90
<i>N</i>	6.00	-3.46			4.09	4.09

energy, giving rise to a large exchange splitting of the conduction band. The localized, majority, Fe_{B1} and Fe_{B2} d states are seen at -12.5 eV, while their unoccupied, minority, states lie just above the Fermi energy, over the range of about 3–4 eV. So, again like in MnFe_2O_4 , we see a large change in the exchange splitting of the conduction band when moving from the inverse to normal spinel structure. For the inverse spinel scenario (*I*) it is of the order of 1.6 eV, while for the normal spinel arrangement it increases to 3.65 eV (Table VII). It is interesting to note, that in the normal spinel structure the sixth localized d electron of the Fe^{2+} ion occupies one of the e_g orbitals, while in the inverse spinel scenario it populates one of the t_{2g} states.

The total spin magnetic moment per formula unit is $4 \mu_B$ (Table V) for all the scenarios studied, with the exception of the normal spinel scenario, where we see a 50% increase to $6 \mu_B$. As all the scenarios give rise to either insulating or half-metallic states, the spin magnetic moments are naturally integer numbers. Table VIII explains how the 50% increase in the total spin magnetic moment comes about when switching from the inverse to normal spinel structure. In the inverse spinel case the spin moment of the tetrahedral Fe ions gets just about cancelled by the spin moment of the $B2$ -octahedral sites, so that the total spin moment is mostly due to the Fe^{2+} ions on the $B1$ sites. In the normal spinel, on the other hand, the spin moment of the tetrahedral Fe^{2+} ions is smaller, and oppositely alligned with the spin moments of the Fe^{3+} ions that occupy all the octahedral sites. Bearing in mind that there are twice as many octahedral sites as the tetrahedral ones, the substantial increase is easy to account for, especially that the induced spin moments on the oxygen sites do not differ much between the two scenarios.

Including spin-orbit coupling for the ground state $I3+$ scenario leads to a very small total orbital moment of about $0.05 \mu_B$ per formula unit, while the total spin moment is very slightly reduced from $4 \mu_B$ to $3.9998 \mu_B$ per formula unit. The orbital moments due to the individual Fe ions are similarly very small, with the tetrahedral Fe being $-0.015 \mu_B$ and the octahedral Fe of $0.035 \mu_B$.

C. CoFe_2O_4

This compound is believed to be mostly of the inverse spinel kind,^{50–52} with divalent Co ions occupying predominantly the octahedral sites. However, similarly to magnetite in the high temperature cubic phase, our calculations find the ground state of CoFe_2O_4 to be half-metallic and of the $I3+$ type (Table II and Fig. 3, center panel). As seen in Table II,

TABLE IX. Spin decomposed exchange splittings of the valence and conduction bands, as well as the energy gaps (in eV), for both inverse and normal spinel structures for CoFe_2O_4 . Here VBM stands for the valence band maximum and CBM for the conduction band minimum, and \uparrow refers to spin-up and \downarrow to spin-down component.

	<i>I</i> scenario	<i>N</i> scenario
VBM \uparrow -VBM \downarrow	0.22	-0.24
CBM \uparrow -CBM \downarrow	1.28	4.07
CBM \uparrow -VBM \uparrow	2.08	4.52
CBM \downarrow -VBM \downarrow	1.02	0.21
Gap	0.80	0.21

the inverse spinel scenario (*I*) is not far, lying only 0.2 eV higher in energy. What this seems to imply is that this compound prefers the inverse arrangement of atoms, independently of the actual valence of the Co ions. The normal spinel solution is about 1.1 eV away. Although the ground state we find is half-metallic, the inverse spinel scenario (*I*), with Co^{2+} ions occupying the *B1* octahedral positions, describes CoFe_2O_4 as an insulator, with a gap of 0.8 eV, which is reduced to 0.21 eV in the normal spinel case (Table IX and Fig. 3). Incidentally, the gap of 0.8 eV for the inverse spinel case compares quite favorably with the LDA+*U* value of 0.63 eV, obtained from a fully relativistic calculation, with *U* of 4.0 eV for Co^{2+} and *U* of 4.5 eV for Fe^{2+} .²⁴

To understand in detail the densities of states in Fig. 3 note that Co has only one minority electron more than Fe. So, the Co^{2+} ion has two localized minority *d* electrons, in addition to the five majority ones. In the ground state *I3+* scenario (center panel in Fig. 3), one of these two minority electrons gets delocalized, contributing to the states at the Fermi energy, while the other, localized, one is seen as a sharp peak just above -10 eV. All the remaining main features of DOS for this scenario are exactly like in the case of *I3+* scenario in magnetite.

For the inverse spinel structure (bottom panel of Fig. 3), the situation is again very much like in magnetite (bottom panel of Fig. 2), with the exception that now we have a small double hump, at about -7 eV, slightly detached from the predominantly O 2*p* valence band, while in magnetite it was still attached to the valence band and represented just a single minority *d* electron.

In the normal spinel scenario the Co^{2+} ions now reside on the tetrahedral sites, with their five localized minority *d* states seen as a rather sharp peak at about -8 eV, in the top panel of Fig. 3. The remaining two localized majority *d* states are sitting just below the majority valence band. All the other features are like in magnetite.

Similarly to other ferrites, one sees substantial change in the exchange splitting of the conduction band between the inverse and normal spinel scenarios, from 1.28 eV to 4.07 eV. Also, the negative spin polarization of the valence band is seen in the normal spinel, while a positive one in the inverse spinel structure. Like in magnetite, for the divalent Co^{2+} ions on the tetrahedral sites in the normal spinel structure, the e_g minority states are populated before

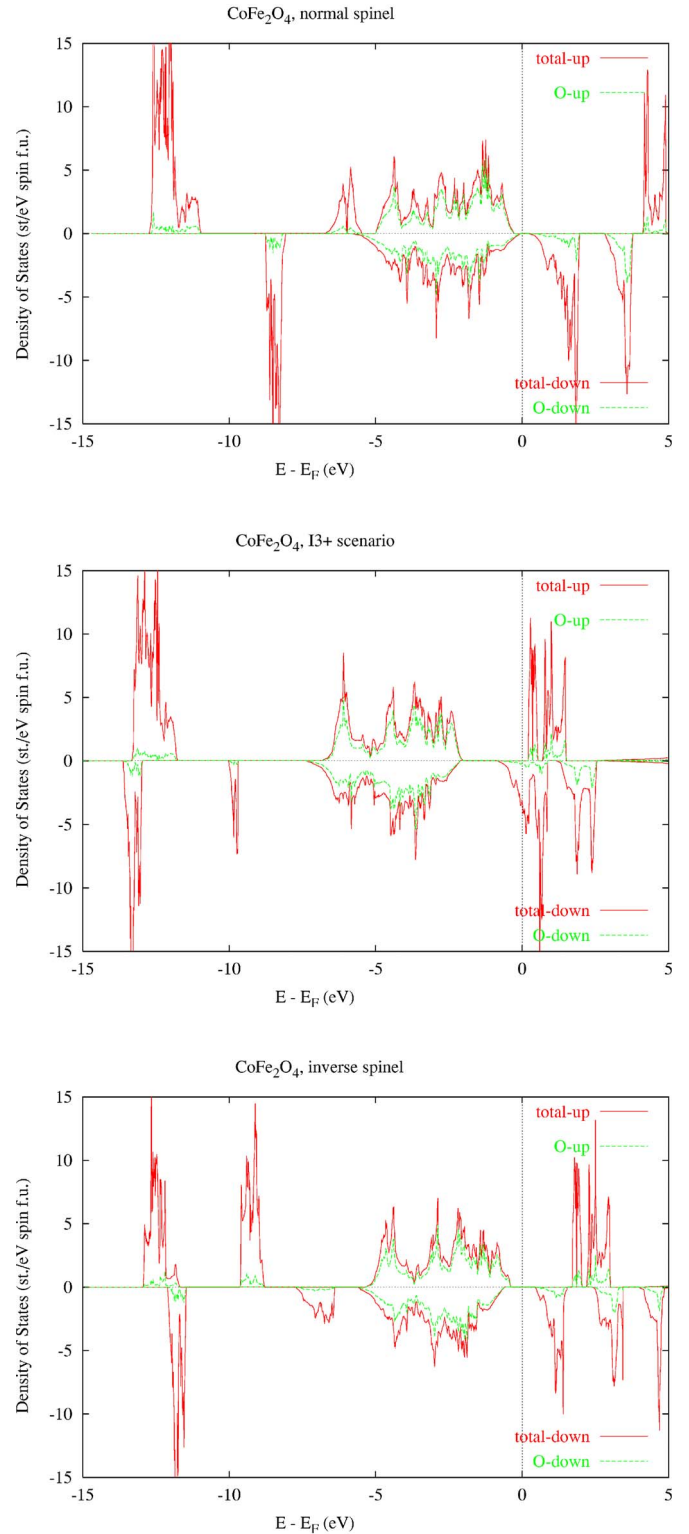


FIG. 3. (Color online) Spin decomposed total densities of states (in red), per formula unit, for CoFe_2O_4 for the normal spinel structure (*N*) (top), for the all 3+ scenario in the inverse spinel arrangement of atoms (*I3+*) (center), and for the inverse spinel scenario (*I*) (bottom). The oxygen contribution to the total density of states is also shown (green dotted lines). The minority DOS is shown on the negative side of the y axis, while the majority contribution is shown on the positive side of this axis.

TABLE X. Type-decomposed spin magnetic moments (in μ_B per formula unit), calculated within SIC-LSD, for CoFe_2O_4 for inverse and normal spinel scenarios. Here A marks the tetrahedral, while $B1$ and $B2$ mark the octahedral sites, and $O1$ and $O2$ stand for two different types of oxygens.

Scenario	Fe_A^{3+}	Co_{B1}^{2+}	Fe_{B2}^{3+}	O1	O2
I	-4.11	2.58	4.11	0.13	0.07
Scenario	Co_A^{2+}	Fe_{B1}^{3+}	Fe_{B2}^{3+}	O1	O2
N	-2.58	4.13	4.13	0.32	0.32

the t_{2g} ones, which is in variance to the inverse spinel structure. In the latter case, the Co^{2+} ions reside on the $B1$ octahedral sites, and the t_{2g} states are lying lower in energy than the e_g states.

As seen in Table V, the total spin magnetic moment for both the I and $I3+$ scenarios is $3 \mu_B$ per formula unit. It is reduced from $4 \mu_B$ in magnetite due to the smaller value of the spin moment of the divalent Co ion of $2.58 \mu_B$ (Table X), in comparison with the spin moment of the divalent Fe ions of $3.57 \mu_B$ (Table VIII). What is however more dramatic is the change of the spin moment when moving from the inverse to the normal spinel arrangement of ions. Table V shows that in the normal spinel scenario the total spin moment is $7 \mu_B$ per formula unit, which again is due to the fact that the octahedral sites are populated exclusively by Fe^{3+} ions, whose spin moments are arranged in parallel to one another and whose magnitudes are considerably larger than the moment of Co^{2+} ions on the tetrahedral sites.

With respect to spin-orbit coupling we find the total orbital moment of the ground state $I3+$ scenario to be quite substantial of the order of $0.58 \mu_B$ per formula unit, and associated mostly with the Co^{3+} ion. As the total spin moment is reduced from $3 \mu_B$ to $2.997 \mu_B$ per formula unit, the ratio of the total orbital to spin moment is 0.19. The ratio of the orbital to spin moment for the Co^{3+} ion itself is 0.21.

D. NiFe_2O_4

NiFe_2O_4 is a ferromagnetic insulator that is of possible interest as a spin filter in MTJs.^{9,10} This compound has the Curie temperature of 850 K, and hence has a great potential for technological applications.

In agreement with experiments, we find the ground state of NiFe_2O_4 to be insulating and of the inverse spinel kind (Table V and the bottom panel of Fig. 4). The calculated energy gap is 0.98 eV (Table XI), in very good agreement with the LDA+ U value of 0.99 eV, obtained assuming U of 4.0 eV for Ni^{2+} and U of 4.5 eV for Fe^{3+} .²⁴ The SIC-LSD gap gets reduced to 0.26 eV in the normal spinel scenario, which is the most energetically unfavorable solution for this compound. In the ground state I scenario, the octahedral $B1$ sites are occupied by Ni^{2+} and $B2$ sites by Fe^{3+} ions, while the tetrahedral sites are populated exclusively by Fe^{3+} ions. Replacing the Co^{2+} ions on the octahedral sites in CoFe_2O_4 by Ni^{2+} leads to the reduction of the total spin magnetic moment of $3 \mu_B$ in CoFe_2O_4 to $2 \mu_B$ in NiFe_2O_4 (Table V),

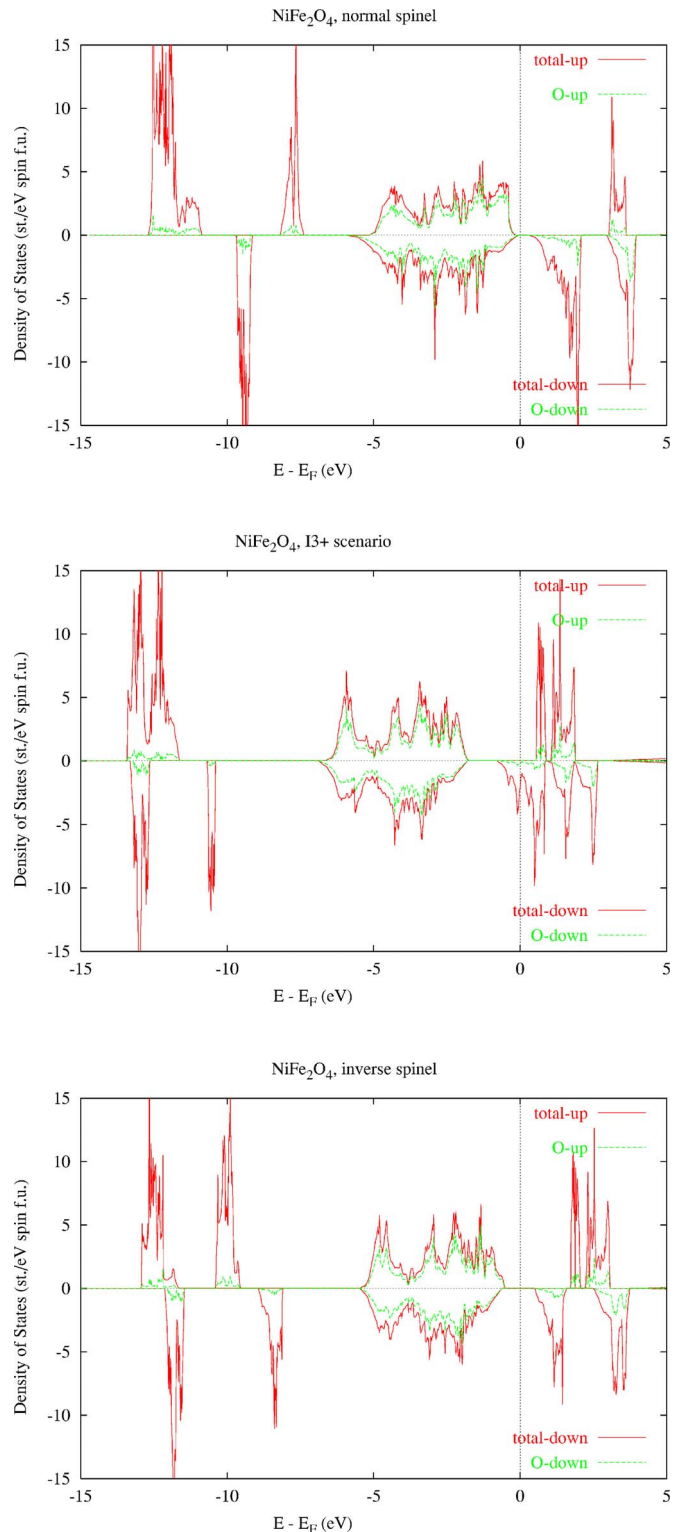


FIG. 4. (Color online) Spin decomposed total densities of states (in red), per formula unit, for NiFe_2O_4 in the normal spinel structure (N) (top), NiFe_2O_4 in the inverse spinel structure for all $3+$ ($I3+$) scenario (center), and NiFe_2O_4 in the inverse spinel structure (I) (bottom). The oxygen contribution to the total density of states is also shown (green dotted lines). The minority DOS is shown on the negative side of the y axis, while the majority contribution is shown on the positive side of this axis.

TABLE XI. Spin decomposed exchange splittings of the valence and conduction bands, as well as the energy gaps (in eV), for both inverse and normal spinel structures for NiFe₂O₄. Here VBM stands for the valence band maximum and CBM for the conduction band minimum, and \uparrow refers to spin-up and \downarrow to spin-down component.

	<i>I</i> scenario	<i>N</i> scenario
VBM \uparrow -VBM \downarrow	0.10	-0.12
CBM \uparrow -CBM \downarrow	1.21	2.93
CBM \uparrow -VBM \uparrow	2.19	3.31
CBM \downarrow -VBM \downarrow	1.08	0.26
Gap	0.98	0.26

since the spin magnetic moment of the Ni²⁺ ion is 1.57 μ_B (Table XII), as compared to 2.58 μ_B spin moment of the Co²⁺ ion (Table X). The oxygen spin moments in both materials are comparable, and aligned in parallel to the cation spin moments on the octahedral sites. The width of the predominantly oxygen 2*p* valence band in NiFe₂O₄ is comparable to the one of CoFe₂O₄, but is reduced with respect to the valence band of magnetite. The reason being that the sixth localized *d* electron of the Fe²⁺ ion [in Fig. 2 (center panel) seen at the bottom of the valence band between -5.0 and -6.0 eV] is strongly hybridized with the oxygen *p* band. The situation is different in NiFe₂O₄, where the three localized minority *t*_{2*g*} electrons, seen at about -8.0 eV (Fig. 4, bottom panel), are well separated from the bottom of the valence band. Also, the exchange splitting of the conduction band, of importance to spin filtering, is about 20% smaller in NiFe₂O₄ than in the Verwey phase of Fe₃O₄.

To understand details of the DOS of the *I*3+ scenario of NiFe₂O₄, it is helpful to follow the discussion of the same scenario for CoFe₂O₄, keeping in mind that a Ni³⁺ ion has two minority *d* electrons in addition to the five majority ones, localized by SIC. Obviously, as already mentioned when discussing MnFe₂O₄, the positions of the localized *d* peaks calculated in the SIC-LSD should not be directly compared with photoemission experiments.⁴¹

The changes in the electronic structure of NiFe₂O₄ when moving from the ground state inverse spinel structure to the normal spinel scenario are immediately obvious from comparing the bottom and top panels of Fig. 4. In the normal spinel case the Ni²⁺ ions occupy the tetrahedral sites, while the octahedral sites are solely taken by the Fe³⁺ ions. As a result, the total spin magnetic moment is increased from 2 μ_B per formula unit to 8 μ_B per formula unit, as seen in Table II, in agreement with experimental findings of Refs. 11 and 12. However, as seen in the top panel of Fig. 4, the density of states is still just insulating in both spin channels. Also, unlike in the case of the inverse spinel structure, the valence band is strongly spin polarized, and the polarization is negative. The oxygen spin magnetic moment is 0.35 μ_B , aligned in parallel to the Fe spin moment (see Table XII), and three times the value it has in the inverse spinel structure. Also, the Ni spin moment is slightly increased in magnitude to -1.65 μ_B . Moreover, the exchange splitting of the conduction band is more than twice increased in the normal spinel, in comparison with the inverse spinel structure, from

TABLE XII. Type-decomposed spin magnetic moments (in μ_B per formula unit), calculated within SIC-LSD, for NiFe₂O₄ for inverse and normal spinel scenarios. Here *A* marks the tetrahedral, while *B1* and *B2* mark the octahedral sites, and O1 and O2 stand for two different types of oxygens.

Scenario	Fe _A ³⁺	Ni _{B1} ²⁺	Fe _{B2} ³⁺	O1	O2
<i>I</i>	-4.11	1.57	4.11	0.14	0.07
Scenario	Ni _A ²⁺	Fe _{B1} ³⁺	Fe _{B2} ³⁺	O1	O2
<i>N</i>	-1.65	4.13	4.13	0.35	0.35

1.21 eV to 2.93 eV. As in the case of the other spinel ferrites in realizing Ni²⁺ ions, the *e*_g states are populated first, i.e., are lying lower in energy than the *t*_{2*g*} states, which is opposite to the inverse spinel structure. However, energetically, the normal spinel structure for NiFe₂O₄ is very unfavorable with respect to the inverse spinel structure (Table II).

Including the spin-orbit coupling for the ground state inverse spinel scenario gives rise to the total orbital moment of 0.67 μ_B per formula unit, and is mostly due to Ni ions, with some minor contributions from Fe atoms. This calculated value is over 2 times larger than calculated from LSD in Ref. 22. Also, in the earlier SIC-LSD calculations for TM oxides Svane and Gunnarsson²⁷ obtained the orbital moment for NiO of 0.27 μ_B , which is substantially smaller than in the present calculations. Since the total spin moment is slightly reduced to 1.9997 μ_B per formula unit, when SOC is taken into account, hence the ratio of the total orbital and spin moments is calculated to be about 0.34. The latter is in good agreement with the experimental estimates of 0.27±0.07 (Ref. 53) and 0.34 (within error bars of up to ±0.11) for Ni in NiFe₂O₄ and NiO.^{53,54} Note that the orbital moment due to the Ni²⁺ ion alone is about 0.7 μ_B , while its spin moment is 1.58 μ_B , both per formula unit, giving rise to the orbital to spin moment ratio of 0.44 for this ion. The total orbital moment is mostly due to the Ni²⁺ ion, as the contributions of other TM ions are smaller by an order of magnitude or so.

V. CONCLUSIONS

We have shown that, owing to a better treatment of correlations, SIC-LSD can provide useful insights to the nature of a number of spinel ferromagnetic insulators. We have been able to address the issues of the normal versus inverse spinel arrangements in these systems, their electronic and magnetic properties and the valence of the transition metal atoms. We find all the studied ferrites to be insulating for both the inverse and normal spinel scenarios, with the calculated energy gaps being smaller in the normal spinel environment, however showing an increasing trend when moving from MnFe₂O₄ to NiFe₂O₄. We have observed dramatic increase of the calculated spin magnetic moments, as well as the exchange splitting of the conduction bands, when moving from the inverse to normal spinel scenarios, some of which have been observed in experiments.¹¹

The total energy considerations seem to favor the inverse spinel arrangement of *TM* ions as the ground state configura-

rations for all the studied ferrites, with the possible exception of MnFe_2O_4 where the normal spinel environment may be preferred, with Mn^{2+} ions on the tetrahedral sites and the Fe^{3+} ions on the octahedral sublattice. Also, based on the total energy arguments, we find a partial delocalization of the minority spin states to be favorable in Fe_3O_4 and CoFe_2O_4 , leading to the half-metallic ground states with all *TM* ions in the trivalent configuration and in the inverse spinel arrangement. The fully inverse spinel scenario, with the Fe^{3+} ions on the tetrahedral sites and the octahedral sites occupied both by

Ni^{2+} ions and Fe^{3+} ions, is found to be the ground state only in NiFe_2O_4 . Finally, these findings constitute a good starting point for further studies, incorporating alloying of the normal and inverse spinel structures.

ACKNOWLEDGMENTS

One of the authors (L.P.) was supported by the Division of Materials Science and Engineering, Office of Basic Energy Sciences, US Department of Energy.

- ¹I. Zutic, J. Fabian, and S. Das Sarma, *Rev. Mod. Phys.* **76**, 323 (2004).
- ²J. M. D. Coey and M. Venkatesan, *J. Appl. Phys.* **91**, 8345 (2002).
- ³S. S. P. Parkin, C. Kaiser, A. Panchula, P. M. Rice, B. Hughes, M. Samant, and S.-H. Yang, *Nat. Mater.* **3**, 862 (2004).
- ⁴S. Yuasa, T. Nagahama, A. Fukushima, Y. Suzuki, and K. Ando, *Nat. Mater.* **3**, 868 (2004).
- ⁵J. S. Moodera, X. Hao, G. A. Gibson, and R. Meservey, *Phys. Rev. Lett.* **61**, 637 (1988).
- ⁶P. LeClair, J. K. Ha, H. J. M. Swagten, C. H. van de Vin, J. T. Kohlhepp, and W. J. M. de Jonge, *Appl. Phys. Lett.* **80**, 625 (2002).
- ⁷V. A. M. Brabers, *Handbook of Magnetic Materials* (1995), Vol. 8.
- ⁸M. Pénicaud, B. Siberchicot, C. B. Sommers, and J. Kübler, *J. Magn. Magn. Mater.* **103**, 212 (1992).
- ⁹U. Lüders, M. Bibes, K. Bouzehouane, E. Jacquet, J.-P. Contour, S. Fusil, J.-F. Bobo, J. Fontcuberta, A. Barthélémy, and A. Fert, *Appl. Phys. Lett.* **88**, 082505 (2006).
- ¹⁰U. Lüders, A. Barthélémy, M. Bibes, K. Bouzehouane, S. Fusil, E. Jacquet, J.-P. Contour, J.-F. Bobo, J. Fontcuberta, and A. Fert, cond-mat/0508764, *Adv. Mater.* (Weinheim, Ger.) (to be published).
- ¹¹U. Lüders, M. Bibes, J.-F. Bobo, M. Cantoni, R. Bertacco, and J. Fontcuberta, *Phys. Rev. B* **71**, 134419 (2005).
- ¹²U. Lüders, G. Herranz, M. Bibes, K. Bouzehouane, E. Jacquet, J.-P. Contour, S. Fusil, J.-F. Bobo, J. Fontcuberta, A. Barthélémy, and A. Fert, *J. Appl. Phys.* **99**, 08K301 (2006).
- ¹³E. J. W. Verwey and P. W. Haayman, *Physica (Utrecht)* **8**, 979 (1941); E. J. W. Verwey, P. W. Haayman, and F. C. Romeijn, *J. Chem. Phys.* **15**, 181 (1947).
- ¹⁴J. P. Wright, J. P. Attfield, and P. G. Radaelli, *Phys. Rev. Lett.* **87**, 266401 (2001).
- ¹⁵V. I. Anisimov, I. S. Elfimov, N. Hamada, and K. Terakura, *Phys. Rev. B* **54**, 4387 (1996).
- ¹⁶V. N. Antonov, B. N. Harmon, V. P. Antropov, A. Ya. Perlov, and A. N. Yaresko, *Phys. Rev. B* **64**, 134410 (2001).
- ¹⁷I. Leonov, A. N. Yaresko, V. N. Antonov, M. A. Korotin, and V. I. Anisimov, *Phys. Rev. Lett.* **93**, 146404 (2004).
- ¹⁸H.-T. Jeng, G. Y. Guo, and D. J. Huang, *Phys. Rev. Lett.* **93**, 156403 (2004).
- ¹⁹G. K. H. Madsen and P. Novak, *Europhys. Lett.* **69**, 777 (2005).
- ²⁰Z. Szotek, W. M. Temmerman, A. Svane, L. Petit, G. M. Stocks, and H. Winter, *Phys. Rev. B* **68**, 054415 (2003).
- ²¹H.-T. Jeng and G. Y. Guo, *J. Magn. Magn. Mater.* **239**, 88 (2002).
- ²²H.-T. Jeng and G. Y. Guo, *J. Magn. Magn. Mater.* **240**, 436 (2002).
- ²³D. J. Singh, M. Gupta, and R. Gupta, *Phys. Rev. B* **65**, 064432 (2002).
- ²⁴V. N. Antonov, B. N. Harmon, and A. N. Yaresko, *Phys. Rev. B* **67**, 024417 (2003).
- ²⁵X. Zuo and C. Vittoria, *Phys. Rev. B* **66**, 184420 (2002).
- ²⁶W. M. Temmerman, A. Svane, Z. Szotek, and H. Winter, in *Electronic Density Functional Theory: Recent Progress and New Directions*, edited by J. F. Dobson, G. Vignale, and M. P. Das (Plenum, New York, London, 1998).
- ²⁷A. Svane and O. Gunnarsson, *Phys. Rev. Lett.* **65**, 1148 (1990).
- ²⁸Z. Szotek, W. M. Temmerman, and H. Winter, *Phys. Rev. B* **47**, 4029 (1993).
- ²⁹P. Strange, A. Svane, W. M. Temmerman, Z. Szotek, and H. Winter, *Nature* **399**, 756 (1999).
- ³⁰J. P. Perdew and A. Zunger, *Phys. Rev. B* **23**, 5048 (1981).
- ³¹O. K. Andersen, *Phys. Rev. B* **12**, 3060 (1975).
- ³²O. K. Andersen and O. Jepsen, *Phys. Rev. Lett.* **53**, 2571 (1984).
- ³³H. L. Skriver, *The LMTO Method*, Springer Series in Solid-State Sciences Vol. 41 (Springer Verlag, 1984).
- ³⁴J. M. Hastings and L. M. Corliss, *Phys. Rev.* **104**, 328 (1956).
- ³⁵G. A. Sawatzky, F. van der Woude, and A. H. Morrish, *Phys. Rev.* **187**, 747 (1969).
- ³⁶L. Braicovich, A. Tagliaferri, G. van der Laan, G. Ghiringhelli, and N. B. Brookes, *Phys. Rev. Lett.* **90**, 117401 (2003).
- ³⁷W. R. L. Lambrecht and O. K. Andersen, *Phys. Rev. B* **34**, 2439 (1986).
- ³⁸A. G. Flores, V. Raposo, L. Torres, and J. Iniguez, *Phys. Rev. B* **59**, 9447 (1999).
- ³⁹A. J. Freeman, B. I. Min, and M. R. Norman, *Handbook on the Physics and Chemistry of Rare Earths*, edited by K. A. Gschneidner, Jr., L. Eyring, and S. Hüfner (North-Holland, Amsterdam, 1987), Vol. 10, pp. 165–229.
- ⁴⁰W. M. Temmerman, Z. Szotek, and H. Winter, *Phys. Rev. B* **47**, 1184 (1993).
- ⁴¹To improve the agreement between the calculated position of the TM *d* states from the SIC-LSD method and the photoemission measurement, one can perform Δ_{SCF} calculations, that is calculations of the total energy difference between two configurations of TM assumed to represent well the initial and final states of a photoemission experiment. This is expressed by the formula $\Delta_{\text{SCF}} = E(d^{n-1}, N_{\text{val}} + 1) - E(d^n, N_{\text{val}})$, meaning that one removes an electron from a TM *d* level and introduces it at the top of the valence band, thus increasing the total number of valence elec-

trons, N_{val} , by 1. Here E represents the total energies of the respective d^{m-1} and d^m configurations. Of course, a problem one faces with this kind of estimate is that the correct final state might not be the ground state of the system with one electron removed. Another way of improving the agreement with spectroscopies is to apply the OEP philosophy. The SIC-LSD method is an orbital dependent density functional theory. Formally, however, SIC-LSD may be viewed as a standard density functional theory, implying that the SIC-LSD energy functional can be represented as a functional of the total charge density alone and minimized with respect to it. This means that there exists an effective Kohn-Sham equation with an effective potential, which is common to all Kohn-Sham states, is self-interaction free and depends only on the total charge density. Here the situation is completely analogous to the optimized effective potential introduced in connection with the Hatre-Fock approximation, (Refs. 42 and 43), for which case the Kohn-Sham eigenvalues are often compared to quasiparticle energies, with a considerable improvement over the Hartree-Fock eigenenergies. Adopting the OEP philosophy, one can search for the effective potential, which reproduces the SIC spin density, and with such a potential derive the density of the localized TM d states. The search may be constrained by looking only for that particular potential shift on the TM sites, which will reproduce the self-consistent TM spin moment of the SIC-LSD calculations.

⁴²J. B. Krieger, Y. Li, and G. J. Iafrate, Phys. Rev. A **45**, 101

(1992); **46**, 5453 (1992); Y. Li, J. B. Krieger, and G. J. Iafrate, *ibid.* **47**, 165 (1993).

⁴³T. Kotani, J. Phys.: Condens. Matter **10**, 9241 (1998).

⁴⁴R. T. Sharp and G. K. Horton, Phys. Rev. **90**, 317 (1953).

⁴⁵J. D. Talman and W. F. Shadwick, Phys. Rev. A **14**, 36 (1976).

⁴⁶M. R. Norman and D. D. Koelling, Phys. Rev. B **30**, 5530 (1984).

⁴⁷F. Walz, J. Phys.: Condens. Matter **14**, R285 (2002).

⁴⁸S. K. Park, T. Ishikawa, and Y. Tokura, Phys. Rev. B **58**, 3717 (1998).

⁴⁹Note that our SIC-LSD calculations for the Verwey scenario and the true low temperature monoclinic phase obtained a gap of ~ 0.1 eV (Ref. 20), which compares well with the experimental value of 0.14 eV (Ref. 48).

⁵⁰R. A. D. Patrick, G. van der Laan, C. M. B. Henderson, P. Kuiper, E. Dudzik, and D. J. Vaughan, Eur. J. Mineral. **14**, 1095 (2002).

⁵¹Y. Waseda, K. Shinoda, and K. Sugiyama, Z. Naturforsch., A: Phys. Sci. **50**, 1199 (1995).

⁵²H. St.-C. O'Neill and A. Navrotsky, Am. Mineral. **68**, 181 (1983).

⁵³G. van der Laan, C. M. B. Henderson, R. A. D. Patrick, S. S. Dhesi, P. F. Schofield, E. Dudzik, and D. J. Vaughan, Phys. Rev. B **59**, 4314 (1999).

⁵⁴V. Fernandez, C. Vettier, F. de Bergevin, C. Giles, and W. Neubeck, Phys. Rev. B **57**, 7870 (1998).